Available online at www.sciencedirect.com
SCIENCE DIRECT
Polymer 47 (2006) 1423–1435
polymer
www.elsevier.com/locate/polymer

Spontaneous polymerization and chain microstructure evolution in high-temperature solution polymerization of *n*-butyl acrylate

Felix S. Rantow [a], Masoud Soroush [a,*], Michael C. Grady [b], Georgios A. Kalfas [b]

[a] *Department of Chemical and Biological Engineering, Drexel University, Philadelphia, PA 19104, USA*
[b] *Marshall Laboratory, E.I. du Pont de Nemours and Company, Philadelphia, PA 19116, USA*

Received 21 August 2005; received in revised form 13 December 2005; accepted 13 December 2005
Available online 19 January 2006

Abstract

This study concerns understanding of the underlying mechanistic pathways in high temperature solution polymerization of *n*-butyl acrylate (*n*BA) in the absence of added thermal initiators. The particular system of interest is the batch polymerization of *n*BA in xylene at temperatures between 140 and 180 °C with initial monomer content between 20 and 40 wt%. A mechanistic process model is developed to capture the dynamics of the polymerization system. Postulated reaction mechanisms include chain-initiation by monomer (self-initiation), chain-initiation by unknown impurities, chain-propagation by secondary and tertiary radicals, intra-molecular chain-transfer to polymer (back-biting), chain-fragmentation (β-scission), chain-transfer to monomer and solvent, and chain termination by disproportionation and combination. The extent of the reactions is quantified by estimating the reaction rate constants of the initiation and the secondary reactions, based on a set of process measurements. The set of measurements considered in the parameter estimation includes monomer conversion, number- and weight-average molecular weights, and average number of chain-branches per chain (CBC). Effect of temperature on chain microstructures was observed to be most evident when microstructures are expressed in terms of their quantities per chain. The evolution of other microstructural quantities such as average number of terminal double bonds per chain (TDBC) and average number of terminal solvent groups per chain (TSGC) was then also investigated. Microstructural quantities per polymer chain (TDBC, TSGC, CBC) are defined based on combinations of ^{13}C, ^{1}H NMR and chromatographic measurements. This study presents (i) a mechanistic explanation for the competing nature of short-chain-branch and terminal double bond formation (i.e. as temperature increases, number of chain branches per chain decreases and number of terminal double bonds per chain increases), (ii) quantitative insights into dominant modes of chain-initiation and chain-termination reactions, and (iii) mechanistic explanations for the observed spontaneous polymerization. The study also reports estimated Arrhenius parameters for second-order self initiation, tertiary radical propagation, secondary radical backbiting and tertiary radical β-scission reaction rate constants. Validation of the mechanistic process model with the estimated Arrhenius parameters and comparison of estimated parameter values to recently reported estimates are also presented.

Keywords: High-temperature free-radical polymerization; Spontaneous polymerization; Mathematical modeling

1. Introduction

High-temperature (ca. above 100 °C) solution polymerization processes have been considered as a viable alternative to produce low solvent-level, high solids-level, environmentally-friendly, acrylic resins [1]. Market competition in industrial resin production has motivated optimal operation of current commercial processes. The optimal operation requires under-standing of how common process variables such as monomer content and reaction temperature influence the final product quality indices.

Recent high-temperature *n*-butyl acrylate (*n*BA) solution homo-polymerization studies have been motivated by the inability of 'classical' chain-polymerization kinetic models (e.g. based on initiation–propagation–termination) in describing *n*BA homo-polymerization at elevated temperatures. This inability has been attributed to significant effects from secondary reactions, such as inter- or intra-molecular chain-transfer reactions, which can lead to branching or scission reactions [2]. Hence recent studies on *n*BA homo-polymerization have focused on (i) the identification of dominant polymerization reactions through spectroscopic methods (i.e. polymer characterization studies) [3–6], (ii) calculation of reaction rate orders [7], (iii) individual estimation of reaction rate constants through pulsed-laser initiated polymerization

* Corresponding author. Tel.: +1 215 895 1710; fax: +1 215 895 5837.
E-mail address: masoud.soroush@drexel.edu (M. Soroush).

0032-3861/$ - see front matter © 2005 Elsevier Ltd. All rights reserved.
doi:10.1016/j.polymer.2005.12.038

(PLP) experiments [8–11], and (iv) simultaneous estimation of a set of reaction rate constants based on advanced (e.g. spectroscopic measurement of the chain branch concentration) and conventional (e.g. gravimetric measurement of polymeric solids content and chromatographic measurement of molecular weight distribution) measurements [2,12].

At first glance, the approach of simultaneously estimating a set of parameters against a set of measurements is the most practical and direct approach toward obtaining a process model. Such approach, however, is often hindered by; (i) non-convexity of the least-squared-error objective function and ill-conditioning of the minimization problem (i.e. more than one set of rate constants can give comparable model predictions), (ii) over- or under-postulation of polymerization reaction networks (i.e. knowledge of dominant reaction pathways is still evolving), (iii) limited availability in number and type of measurements. Consequently, recent research directions in this area have included (i) identification of novel 'experimental sensors' (measurements) to be included in the parameter estimation [12], (ii) identification of optimal parameter-measurement pairs through sensitivity analyses in order to reduce the complexity of the parameter estimation problem [13,14] and (iii) use of global optimization approaches to obtain a unique set of rate constants (e.g. implementation of the simulated annealing algorithm in modeling package PREDICI® [15]).

Hence an alternative to reducing complexities in the model building and the parameter estimation problem is the inclusion of spectroscopic measurements. The inclusion should limit the number of different combinations of rate constants that can give (i) comparable model predictions and (ii) satisfactory predictions for all type of measurements. The availability of these measurements depends on the observability of signature peaks that can be used as a measure of a certain chain microstructure quantity. Particularly in polymer characterization problems, of critical importance is the observance of peaks that are distinguishable from others arising from polymeric backbone atoms. The complexity of the simultaneous parameter estimation problem is also reduced by the more reliable knowledge of the dominant reaction rate constants (e.g. linear propagation and termination) obtained from PLP experiments.

This study is motivated by the observation of near-complete conversion polymerization experiments that were carried out in the absence of thermal initiators [16]. Spectroscopic evidence (ESI-FTMS) of the absence of initiator moieties in the polymer chains that are produced from the spontaneous *n*BA polymerization experiments [17] further supports this observation. In addition to the spontaneous polymerization observed at high temperatures (ca. above 140 °C), secondary reactions occurring at these temperatures are also studied. The aims of this study are (i) to gain insight into initiation mechanism and to probe the significance of the initiation reaction, (ii) to quantitatively explain the effects of process variables on polymer quality indices (conversion, molecular weight, chain microstructures). The understanding of the initiation and secondary mechanisms can potentially lead to initiator-free commercial polymerization processes and can help process engineers in the safety assessment of high-temperature polymerization processes.

Section 2 describes the experimental and analytical procedures, and Section 3 describes the postulation of the polymerization reaction network. The parameter estimation approach used in this study is introduced in Section 4. Discussions and analyses of results are presented in Section 5, followed by concluding remarks in Section 6. Derivation of the process model is presented in the Appendix A.

2. Experimental and analytical procedures

n-Butyl acrylate (BASF, 99.5%, with boiling point of 146.8 °C) was passed through an inhibitor removal column (DHR-4, Scientific Polymer Products, Inc.) prior to use. Xylene (ExxonMobil Chemical Co., an 80/20 mix of xylene isomers and ethyl benzene with a boiling point range of 137–143 °C) and 4-methoxyphenol (99%, ACROS, with boiling point of 243 °C) were used as received. Polymerizations were carried out in a 1-l glass RC1 calorimeter-reactor (Mettler-Toledo GmbH, Schwerzenbach, Switzerland).

Each experiment started with loading the xylene solvent into the reactor. Nitrogen gas was subsequently purged through the solvent and reactor for 15–30 min. The monomer was then pumped into the reactor and heated under nitrogen blanket to the desired reaction temperature. Reaction temperature was maintained throughout the course of the polymerization by adjustment of the reactor jacket temperature. Samples drawn from the reaction mass at specified time intervals were diluted (50/50 v/v) in a cold inhibitor solution (1000 ppm 4-methoxy phenol in xylene) to prevent further reaction from taking place.

Polymer and residual monomer concentrations were determined by gravimetric and chromatographic (GC) analyses, respectively. GC analyses were carried out by using Hewlett–Packard (HP) 6890 GC-FID system with a 30 m DB-5 separation column. The FID (flame ionization detector) temperature was set to 250 °C, with oven temperature ramp at 10 °C/min. Measurement of residual monomer by weight was obtained from the integration of monomer peak area, adjusted with a dilution factor when necessary.

Molecular weight distributions were determined by using an HP 1090 HPLC (high performance liquid chromatography) system, equipped with an HP 1047A RI (refractive index) detector and a four-column set configuration (10^5, 10^4, 10^3, 10^2 Å 30 cm × 7.8 mm id microstyragel columns). Tetrahydrofuran was used as the mobile phase at flow rate of 1 mL/min at 40 °C. Data from the RI detector was collected and processed by using a Waters Millennium system. Narrow molecular weight polystyrene standards were used to calibrate the column set.

Polymeric solid samples for NMR analyses were isolated through high vacuum and evaporation at 65 °C. Quantitative carbon and proton NMR spectra were recorded at 34 °C on a Bruker DRX-400 MHz spectrometer (^{1}H frequency of 400.13 MHz and ^{13}C frequency of 100.62 MHz). Deuterated chloroform ($CDCl_3$) was used as solvent in all analyses. ^{13}C

NMR spectra were obtained by using a 10 mm broadband probe equipped with ^{1}H decoupler, acquisition time of 1.36 s, spectral width of 24 kHz, relaxation time of 15 s, number of scans between 1600 and 3200, and a 90° pulse width of 13.9 μs. ^{1}H NMR spectra were obtained by using a 4 s acquisition time, a 10 kHz spectral width, an 8 s relaxation time, number of scans of 16 and an 11.5 μs 90° pulse width. Peak assignments obtained through analyses of DEPT spectra reported by [17] is used in this study.

3. Postulation of reaction network

3.1. Chain-initiation

Studies in spontaneous polymerization of methyl methacrylate (MMA) have cited both self-initiation [18–24] and decomposition of impurities, i.e. oxygen or peroxides in general [25,26], as the underlying mechanism for the generation of initiating radicals. In a recent study on thermally-initiated MMA polymerization, it is reported that MMA could also undergo reaction with air to form macromolecular peroxides [27]. Both peroxide decomposition [28] and self-initiation [29] have been assumed to be responsible for the generation of initiating radicals in *n*BA polymerization. In this study, mechanisms of thermal self-initiation proposed for methyl methacrylate [22] and the decomposition of peroxide [30] are adopted for *n*BA. The initiation step dictates the amount of live radicals (initially) present, and will eventually dictate the amount of dead polymer chains formed. The initiating radicals formed by the peroxide decomposition is represented by live radical chains of length zero (P_0). While in the self-initiation reaction, the initiating radicals are assumed to be the monomer itself, thus represented as live (secondary) radical chains of length one (P_1).

3.2. Chain-propagation, chain-transfer to polymer and chain-fragmentation

Intra-molecular chain-transfer to polymer or backbiting has been postulated to dominate at lower monomer content (ca. below 50 wt%) [2], and is known to occur even at lower temperatures [8,31]. The backbiting event allows for the creation of short chain-branches, upon propagation of the tertiary (mid-chain) radical near the end of the chain. This tertiary radical can alternatively undergo β-scission, to create a dead polymer chain with a terminal double bond (TDB) and a live polymer chain. As only averages are considered in this study, only the scission reactions, which create long dead chains instead of dead trimer chains with TDBs are included in the overall kinetic scheme. The propagation, chain transfer to polymer, branching and scission reactions are presented in unison, since these reactions simultaneously affect the average molecular weights, the number of TDBs and the number of branching points. Dead polymer chains are created through the scission reaction, and are governed by the amount of tertiary radicals (Q_n) present. The scission reaction leads to the creation of a dead polymer chain (D_{n-2}) with a TDB in one step. At the same time the tertiary radicals can also form chain branches through further propagation. SCB denotes a short chain-branch point formed through such a reaction.

3.3. Chain-transfer to monomer and solvent

Chain transfer to monomer allows for the creation of a dead chain with a TDB and a live chain. The rate of chain transfer to monomer is influenced by the amount of monomer and live (propagating) chains present at a given time. The concentration of monomer is much larger compared to the concentration of live chains. The significance of chain transfer to monomer, however, is often discounted due to the low reaction rate constant relative to the scission reaction. A recent estimation of the rate constant for chain transfer to monomer reactions in high-pressure high-temperature polymerization of *n*BA indicated that transfer to monomer might have a more significant contribution towards the overall kinetic scheme [12]. In this study, since temperature effects on the number of terminal double bonds are of interest, β-scission and chain transfer to monomer reactions are considered in the model development. Along with chain transfer to monomer [32], *n*BA has also been reported to undergo chain transfer to solvent [6,33]. Upon chain-transfer to monomer, a live secondary radical of length one or the monomer itself (P_1^{TDB}) is created. When this radical propagates further, a TDB is created for the resulting chain. The reactive solvent species (i.e. in this study. xylol radical) is represented as a live chain of length zero (P_0), and is assumed to propagate at the same rate as a secondary radical.

Table 1
Postulated polymerization reaction network for batch polymerization of *n*BA in xylene at 140–180 °C with a monomer content of 20–40 wt%

$2M \xrightarrow{k_{ti}} 2P_1$
$R_1\text{–O–O–}R_2 \xrightarrow{k_{O_2}} 2P_0$
$P_n + M \xrightarrow{k_p} P_{n+1}$
$P_n \xrightarrow{k_{bb}} Q_n$
$Q_n + M \xrightarrow{k_{pq}} P_{n+1}(+\text{SCB})$
$Q_n \xrightarrow{k_\beta} D_{n-2} + P_2(+\text{TDB})$
$P_n + M \xrightarrow{k_{tm}} D_n + P_1^{TDB}$
$P_1^{TDB} + \text{M} \xrightarrow{k_p} P_2(+\text{TDB})$
$P_n + S \xrightarrow{k_{ts}} D_n + P_0$
$P_n + P_m \xrightarrow{k_{tc}^{sec-sec}} D_{n+m}$
$P_n + P_m \xrightarrow{k_{td}^{sec-sec}} D_n + D_m$
$P_n + Q_m \xrightarrow{k_{tc}^{sec-tert}} D_{n+m}$
$P_n + Q_m \xrightarrow{k_{td}^{sec-tert}} D_n + D_m$
$Q_n + Q_m \xrightarrow{k_{tc}^{tert-tert}} D_{n+m}$
$Q_n + Q_m \xrightarrow{k_{td}^{tert-tert}} D_n + D_m$

The subscripts represent polymer chain length.

3.4. Chain-termination

While termination for acrylates usually take place almost exclusively by combination, at high temperatures, the extent of termination by disproportionation can increase [34,35]. It is assumed that termination occurs by a combination of both modes, and the estimates reported in [2] on the relative extent of each termination mode are used in this study to describe the various termination reactions.

The postulated polymerization reaction network is presented in Table 1. Details of the derivation of the batch polymerization process model is presented in the Appendix A.

4. Parameter estimation

The objective of the parameter estimation is to obtain reliable estimates for spontaneous initiation and secondary reaction rate constants. The rate constants are simultaneously estimated from a set of measurements. Two different sets of measurements at two different temperatures are considered in the parameter estimation.

A simultaneous parameter estimation problem with a sum of squared errors (between model predictions and measurements) performance index is formulated. The simplex search method (fminsearch) of the optimization toolbox of the commercial software MATLAB version 6, is used in the parameter estimation. The parameter non-negativity constraint is implicitly imposed in the simplex method by estimating the exponents of the parameters to be estimated (i.e. estimate $\hat{\theta}$, where $\theta = 10^{\hat{\theta}}$, instead of directly estimating θ, where θ is the rate constant actually being estimated). It was observed that, by estimating the exponents instead of the actual parameters, the algorithm converges faster to a minimum. To minimize the probability of obtaining a local minima, different initial conditions for the parameter estimates were used in the parameter estimation. Rate constants for the primary reactions available in the literature are not re-estimated and are used in the model. The minimization problem is of the form

$$\min_{\hat{\theta}} J = \sum_{i=1}^{5} \sum_{j=1}^{N_i} \left[\frac{y_i(t_j) - \hat{y}_i(t_j)}{\hat{y}_i(t_j)} \right]^2$$

where $y_1,\ldots,y_4$ represent the measurements of monomer conversion (X), number-average molecular weight (M_n), weight-average molecular weight (M_w), and number of (short) chain branches per chain (CBC), respectively. N_i is the number of measurements of the measured variable y_i, and the parameters being estimated $\theta_1,\ldots,\theta_4$ are the rate constants corresponding to the second-order self-initiation (k_{ti}), propagation of tertiary radicals (k_{pq}), secondary radical backbiting (k_{bb}), and tertiary radical β-scission (k_β). The measurements were obtained at temperatures of 160 and 180 °C, each at an initial monomer content of 40 wt%. The parameters k_p, k_{tm}, k_{ts}, k_t were extrapolated from Refs. [8,11,32,33], respectively. It was assumed that the combination of measurements X, M_n, M_w, CBC, contains adequate information for the estimation of the rate constants: k_{ti}, k_{pq}, k_{bb}, k_β. The relationship between the rate constants and the set of measurements can be seen by inspection of the analytical model structure (Appendix A): the measurement of X is directly influenced by k_{ti} (mass balance equation on monomer), CBC is directly influenced by k_{pq} (mass balance equation on chain branches), and the average

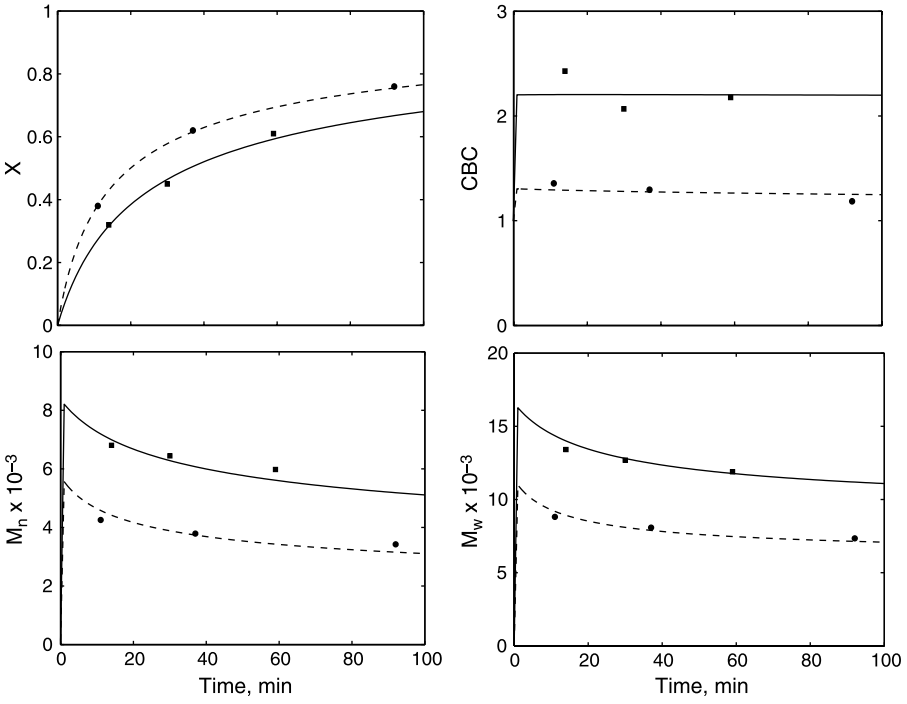

Fig. 1. Quality of fit for parameter estimation based on measurements of X, M_n, M_w and CBC. Solid square and circle markers represent experimental data at 160 and 180 °C, with initial monomer content of 40 wt%, respectively. Solid and dashed lines represent model predictions at 160 and 180 °C, with initial monomer content of 40 wt%, respectively.

Table 2
Estimated rate constant values based on measurements of X, M_n, M_w, and CBC at 160 and 180°C, at an initial monomer content of 40 wt%, and the corresponding Arrhenius parameters

Rate constant	160 °C	180 °C	A	E (J mol^{-1})
k_{ti} (L mol^{-1}s^{-1})	1.25×10^{-6}	3.05×10^{-6}	8.27×10^{2}	73,152
k_{pq} (L mol^{-1}s^{-1})	5.16×10^{1}	5.20×10^{1}	5.99×10^{1}	534
k_{bb} (s^{-1})	1.92×10^{4}	2.42×10^{4}	3.87×10^{6}	19,114
k_{β} (s^{-1})	7.40×10^{-1}	4.42×10^{0}	2.88×10^{17}	145,853

molecular weights are indirectly influenced by all the parameters being estimated. Experimental trends to be captured in the parameter estimation are: increasing monomer conversion, decreasing average molecular weights and CBC, with increasing temperature. Monomer conversion and molecular weight measurements were obtained through gravimetric and chromatographic measurements, respectively.

The measurements of number average of chain branches per chain (CBC) were obtained by using quantitative *n*BA ^{13}C NMR peak area at 47–49 ppm as a measure of number of branch points (quaternary carbon atom [3]) and the peak area at 165–180 ppm (carbon atom on C=O [17]) or the peak area at 65 ppm (carbon atom on C–O [17]) as a measure of number of repeat units. One way to report number of branches is to use the ratio of number of branches to number of repeat units. When this ratio is multiplied by 100, the number of branches is expressed as (average) number of branch points per 100 repeat units (CBH). The effect of temperature on chain branches was most evident as the quantity CBC is defined as:

$$\mathrm{CBC} = \left(\frac{\mathrm{SCBH}}{100}\right)\mathrm{DP}_n$$

where DP_n is the number-average degree of polymerization. The quality of fit at the two different temperatures is presented in Fig. 1. Estimates at each temperature, and the corresponding estimates of the Arrhenius parameters are presented in Table 2. To gauge the performance of the simplex search algorithm, the surface of the objective function is presented as functions of k_{ti} and k_{bb}, at 160 °C and initial monomer content of 40 wt% in Fig. 2. The parameters k_{ti} and k_{bb} represent the two underlying pathways that directly influences all of the measurements (terms in the rate laws that include k_{pq} and k_{β} depend on amount of tertiary radicals, which is directly governed by the rate of backbiting). Assuming that the intervals considered for k_{ti} and k_{bb} are sufficiently large, it is shown that the global minima was obtained by using the optimization approach (k_{ti} = 1.25×10^{-6} L mol^{-1} s^{-1}, k_{bb} = 1.92×10^{4} s^{-1}).

5. Discussions and analyses

5.1. Parameter estimation results and model validation

From Fig. 1, it is shown that a satisfactory fit was obtained. Based on the parameter estimates at the two different temperatures, Arrhenius parameters were estimated and are presented in Table 2. Calculated secondary reaction parameter values (based on the estimated Arrhenius parameters) were then compared with literature values at temperatures 140 and 170 °C. The comparison is presented in Table 3. Note that the nominal values of k_{pq} and k_{bb} are in agreement with reported values. There is a discrepancy over literature values for the value of k_{β}, particularly with that reported in [12]. It should be noted that the simultaneous parameter estimation study in [12] considers different sets of measurements, parameters and reaction paths (e.g. formation of long chain branches preceded by intermolecular chain transfer is considered). As will be discussed further in the following subsection, the observed trend of chain branches vs. number average degree of polymerization suggests the formation of short chain branches, as opposed to long ones. The estimate for k_{ti} is the first report on the postulated second-order self-initiation reaction. The apparently high energy activation value for k_{β} is currently understood as a high

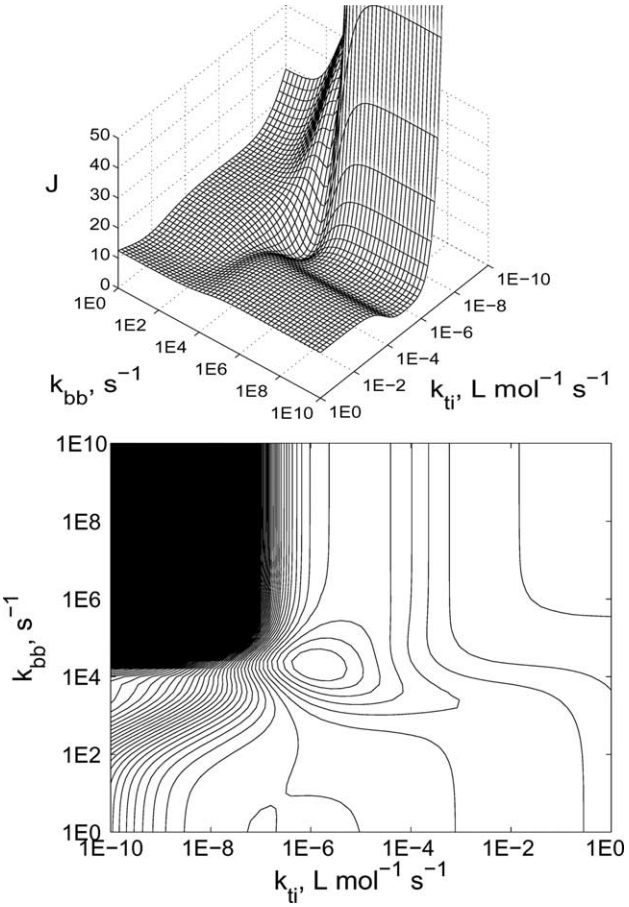

Fig. 2. Surface of the objective function (sum of squared error between model predictions and measurements of monomer conversion, number-average molecular weight, weight-average molecular weight and number-average chain branches per chain) of the parameter estimation as functions of k_{ti} and k_{bb} at 160 °C, initial monomer content of 40 wt%.

Table 3
Reported and estimated rate constant values for high-temperature *n*BA polymerization

Rate constant	A	E (J mol^{-1})	140 °C	170 °C	Ref.
k_{ti} (L mol$^{-1}s^{-1}$)	8.27×10^{2}	73,152	4.66×10^{-7}	1.97×10^{-6}	This study[a]
k_p, (L mol^{-1}s^{-1})	2.21×10^{7}	17,900	1.21×10^{5}	1.91×10^{5}	[8]
	–	–	–	1.67×10^{5}	[12]
k_{pq} (L mol^{-1}s^{-1})	$k_p\times1.2\times10^{-3}$	–	1.45×10^{2}	–	[2]
	5.99×10^{1}	534	5.13×10^{1}	5.18×10^{1}	This study
k_{tm} (L mol^{-1}s^{-1})	$k_p\times1.60\times10^{-2}$	15,200	2.31×10^{1}	4.43×10^{1}	[32]
	–	–	–	1.81×10^{5}	[12]
k_{ts} (L mol^{-1}s^{-1})	$k_p\times1.95\times10^{1}$	32,175	2.01×10^{2}	5.39×10^{2}	[33]
k_{bb} (s^{-1})	3.50×10^{7}	29,300	6.91×10^{3}	1.23×10^{4}	[38]
	–	–	–	2.13×10^{4}	[12]
	–	–	4.00×10^{3}	–	[2]
	3.87×10^{6}	19,114	1.48×10^{4}	2.16×10^{4}	This study
k_{tp} (L mol^{-1}s^{-1})	–	–	–	5.00×10^{3}	[12][b]
k_β (s^{-1})	–	–	6.00×10^{0}	–	[2]
	–	–	–	6.28×10^{4}	[12]
	2.88×10^{17}	145,853	1.04×10^{-1}	1.85×10^{0}	This study
k_t (L mol^{-1}s^{-1})	2.57×10^{8}	5,590	5.05×10^{7}	5.64×10^{7}	[11]
	–	–	–	1.10×10^{7}	[12]

[a] The self initiation rate constant was estimated while assuming that initiation by impurities did not occur.
[b] Inter-molecular chain transfer to polymer was not considered in this study.

temperature phenomenon, as scission is not observed to be prevalent at lower reaction temperatures.

To quantify the reliability or variability of the reported estimates, we consider the local sensitivity of the parameters with respect to the measurements (we assume that the parameters are linearly related to the measurements within one order of magnitude of the nominal values). The parameter-measurement sensitivity, with respect to measurements of monomer conversion and weight-average molecular weight, is presented in Table 4. The variability of the estimates can then be calculated as follows:

$$\Delta\theta_{\text{experimental}} = \left(\frac{\Delta\theta}{\Delta y}\right)_{\text{theoretical}} \Delta y_{\text{experimental}}$$

hence a conservative approach towards quantifying the variability of the reported estimates is by using measurement with the largest variability (e.g. monomer conversion, $\pm10\%$ off the average) as basis for the above calculation. By using such approach, the variabilities with respect to the nominal values at 160 °C are approximately: $k_{ti}\times5\geq k_{ti}\geq k_{ti}\div3$, $k_{pq}\times5\geq k_{pq}\geq k_{pq}\div2$, $k_{bb}\times3\geq k_{bb}\geq k_{bb}\div2$ and $k_\beta\times60\geq k_\beta\geq k_\beta\div60$.

Table 4
Local sensitivity of parameter-measurement with respect to nominal parameter and measurement values at 160 °C, 200 min reaction time and initial monomer content of 40 wt%

Parameter (θ)	$\Delta\theta$	ΔX (%)	ΔM_w (%)
k_{ti}	$\times10$	+17.75	−46.54
	$\div10$	−26.49	+96.48
k_{pq}	$\times10$	+19.50	−123.89
	$\div10$	−19.72	+53.79
k_{bb}	$\times10$	−34.90	−81.95
	$\div10$	+19.57	+129.49
k_β	$\times10$	+1.48	−11.44
	$\div10$	−0.15	+1.40

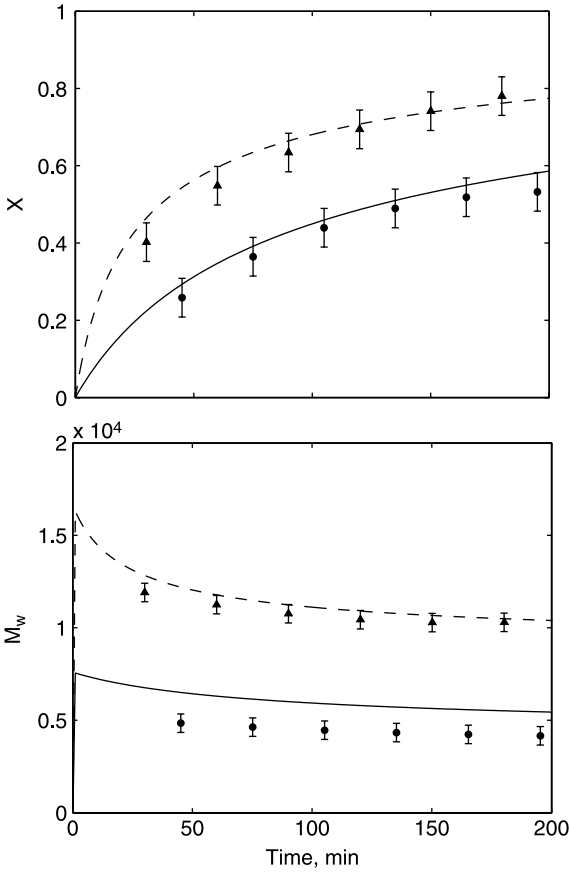

Fig. 3. Model predictions vs. experimental data for X and M_w, predictions are based on estimated Arrhenius parameters (Table 2). Solid triangle and circle markers represent experimental data with initial monomer content of 20 and 40 wt%, at 160 °C, respectively. Solid and dashed lines represent model predictions at initial monomer content of 20 and 40 wt%, at 160 °C, respectively.

The model was then validated by comparing model predictions with experimental data at extrapolated conditions (at experimental conditions outside the range used in the parameter estimation). In Fig. 3, the model predictions are compared against experimental data at 160 °C, and at initial monomer content of 20 wt% (the model was based on subset of data obtained at 160–180 °C, initial monomer content of 40 wt%). From separate triplicate experiments, it was observed that the variability of the monomer conversion data can be captured by using constant error bars on the average value. The constant error bars represent ±10% off the average for the monomer conversion data and represent ±5% off the average for the weight-average molecular weight data. The comparison shows that the model was able to capture the monomer conversion trend quantitatively and the weight-average molecular weight trend qualitatively (slight over-prediction). Similarly, the model predictions are compared with experimental data at 140 °C, at initial monomer content of 40 wt%. The comparisons are presented in Fig. 4. The model was over-predicting the extent of monomer conversion at 140 °C, and slightly under-predicting the weight-average molecular weight profile. To understand the cause of the discrepancies, the model was then validated against molecular structure quantities as function of temperature. This validation is presented in Fig. 5. From the figure, it is shown that the model is able to capture the temperature-chain branch trend, however, is not able to capture the temperature-terminal double bond trend. This suggests that the model has not fully captured the interplay between the chain branch and terminal double bond formation. This also explains the high variability of the estimate for k_β. It should also be mentioned that many efforts have been focused on understanding the effects of chain length on the termination rate coefficient [36]. In this study, it is assumed that the rate of chain-termination does not depend on chain length at low initial monomer content (shorter polymer chains throughout reaction time). The rate constant for chain-termination is, therefore, not re-estimated, instead, the chain termination parameters reported in [2] is adopted.

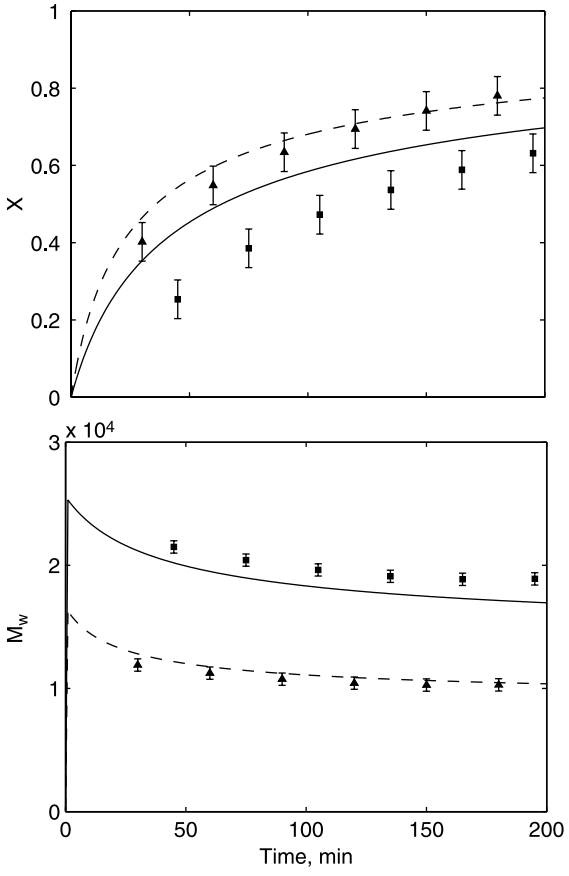

Fig. 4. Model predictions vs. experimental data for X and M_w, predictions are based on estimated Arrhenius parameters (Table 2). Solid triangle and circle markers represent experimental data at 140 and 160 °C, respectively, with initial monomer content of 40 wt%. Solid and dashed represent model predictions at 140 and 160 °C, respectively, with initial monomer content of 40 wt%.

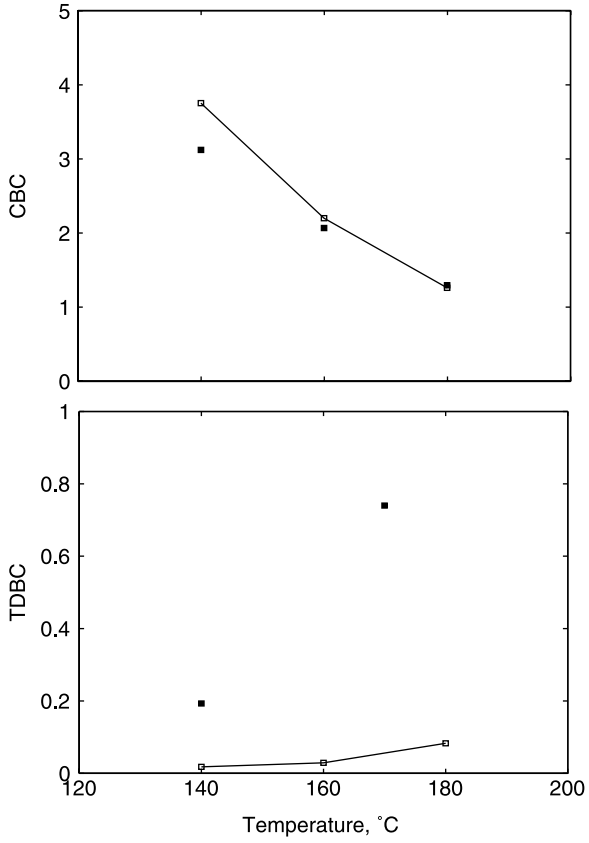

Fig. 5. Model predictions vs. experimental data for TDBC and CBC vs. temperature, predictions are based on estimated Arrhenius parameters (Table 2). Solid markers represent experimental data. Experimental data at 160, 170 and 180 °C correspond to initial monomer contents of 40, 33, and 40 wt%, respectively (batch), at reaction time of ca. 40–50 min. The experimental data at 140 °C has a final monomer content of ca. 50 wt% (starved-feed, 90 min feed time), at reaction time of 90 min. The experimental data at 140 °C is recalculated from [2]. Empty markers represent batch model predictions at ca. 60 min reaction time, and the solid lines are plotted only to connect the model predictions.

5.2. Microstructural evolution and dominant modes of chain-initiation and chain-termination

In this study, temperature was found to have the largest effect on microstructures, and this effect was most evident

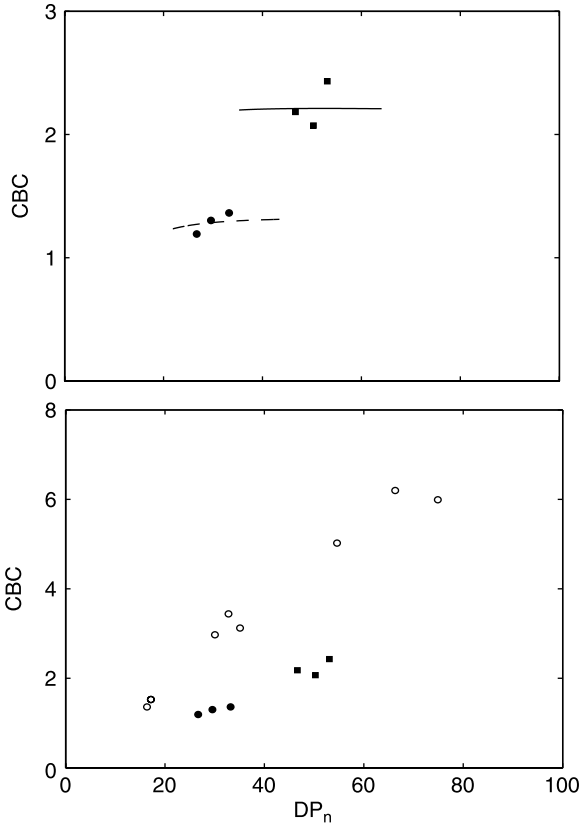

Fig. 6. (Top) Model predictions vs. experimental data for CBC, predictions are based on estimated Arrhenius parameters (Table 2). Solid square and circle markers represent experimental data at 160 and 180 °C, with initial monomer content of 40 wt%, respectively. Solid and dashed lines represent model predictions at 160 and 180 °C, with initial monomer content of 40 wt%, respectively. (Bottom) Experimental trends of CBC. The empty circles are reproduced from [2], based on 140 °C starved-feed *n*BA-xylene experiments. Solid circles are experimental data from this study, based on 160–180 °C batch polymerization experiments.

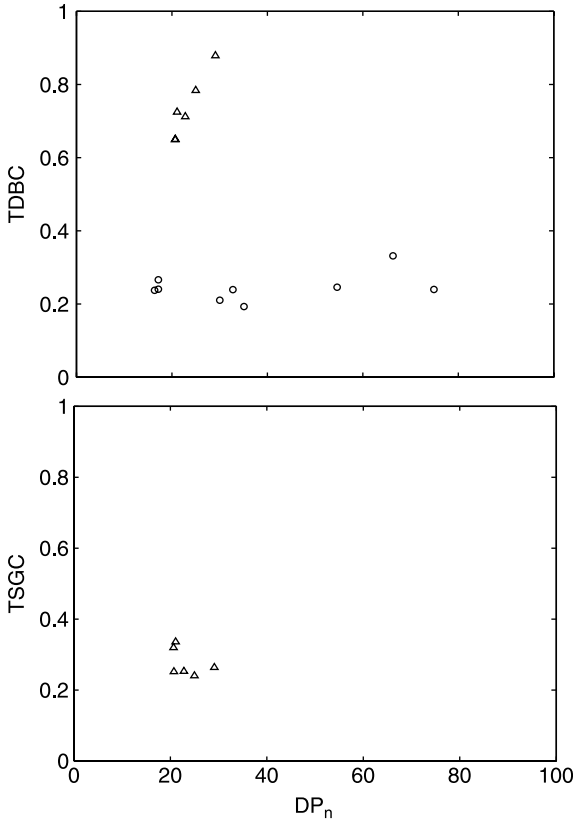

Fig. 7. Experimental data for TDBC and TSGC. The empty circles are reproduced from [2], based on 140 °C starved-feed *n*BA-xylene experiments. Empty triangles are experimental data from this study, based on 170 °C batch polymerization experiments, with initial monomer content of 33 wt%.

when microstructural quantities are represented as quantities per chain. The linear increase of average number of chain branches per chain as a function of DP_n (Fig. 6) suggests the formation of short chain branches and confirms the reaction network postulated in [2]. This trend suggests a constant 'rate of formation' of chain branches (i.e. if there is a shift from intra- to inter-molecular chain transfer, the 'rate of formation' should not be constant as DP_n increases). This also supports studies that attribute the (short) chain branch formation to backbiting. Data from [2], recalculated and presented in Fig. 6, also support this observation.

Fig. 7 presents the microstructural data of number-average terminal double bonds per chain (TDBC) and number-average terminal solvent groups per chain (TSGC). TDBC and TSGC measurements were obtained from quantitative *n*BA ^{1}H NMR analyses. The ^{1}H NMR peak area at 5.5 and 6.2 ppm (two hydrogen atoms on the terminal double bond [4]) was used as a measure of the concentration of terminal double bonds, and the peak area at 7.1 ppm (four hydrogen atoms on the terminal solvent group [17]) was used as a measure of the concentration of terminal solvent groups. Number of repeat units was measured by using the peak area at 4.1 ppm (two hydrogen atoms on CH2 next to COO [17]). Number of terminal double bonds per 100 repeat unit (TDBH) was calculated by dividing the peak area at either 5.5 or 6.2 ppm by half of the peak area at 4.1 ppm, multiplied by 100; and the number of terminal solvent groups per 100 repeat unit (TSGH) by dividing one-fourth of the peak area at 7.1 ppm by half of the peak area at 4.1 ppm, multiplied by 100. Similarly, the number of terminal double bonds per chain (TDBC) and the number of terminal solvent groups per chain (TSGC) are given by:

$$\mathrm{TDBC} = \left(\frac{\mathrm{TDBH}}{100}\right)\mathrm{DP}_n$$

$$\mathrm{TSGC} = \left(\frac{\mathrm{TSGH}}{100}\right)\mathrm{DP}_n$$

At the moment there is not enough data to draw conclusions on the evolution of terminal solvent groups per chain, however, the values of TSGC agree with previous studies. FTMS studies by Grady et al. [1], Peck and Hutchinson [6] and Quan et al. [17] reported that at elevated temperatures most of chains are xylol-initiated or β-scission initiated/terminated. Experimental trends show that approximately 3 out of 10 chains are xylol-initiated, and 7 out of 10 chains

Table 5
Rate constant values for decomposition of oxygen and peroxides [30], used in simulations presented in Fig. 8

Type of impurity	A	E (J mol^{-1})	Value at 160 °C (s^{-1})
Oxygen (O_2)	6.00×10^{9}	116,000	6.15×10^{-5}
Di-*t*-butyl peroxide (DTBP)	6.64×10^{15}	156,000	1.02×10^{-3}
Di-cumyl peroxide (DCP)	1.12×10^{18}	170,000	3.53×10^{-3}
t-Butyl perisopropyl carbonate (TBPC)	1.42×10^{15}	141,000	1.41×10^{-2}

are β-scission terminated at 170 °C and at initial monomer content of 33 wt% (Fig. 7). A more thorough study on the evolution of chain microstructures for broader experimental ranges of temperature and monomer content is currently being carried out.

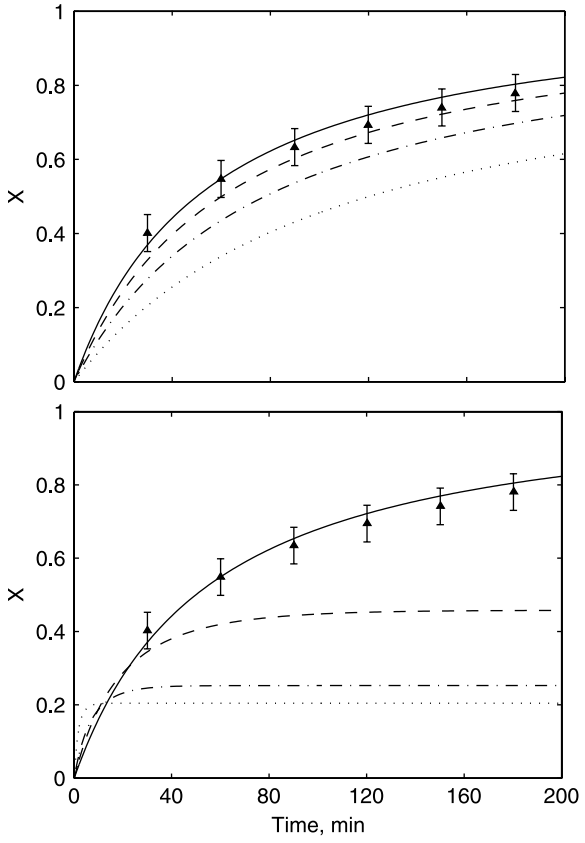

Fig. 8. (Top) Model predictions vs. experimental data for monomer conversion, *X*, predictions based on oxygen-initiated polymerization (no self-initiation), with rate constants given in Table 4. Solid triangle markers represent experimental data at 160 °C, with initial monomer content of 40 wt%. Solid, dashed, dash–dotted and dotted lines represent model predictions for oxygen-initiated polymerization with initial oxygen amount of 800, 600, 400 and 200 ppm, at 160 °C and initial monomer content of 40 wt%, respectively. (Bottom) Model predictions vs. experimental data for *X*, predictions based on impurity-initiated polymerization (no self-initiation), with rate constants given in Table 4. Solid triangle markers represent experimental data at 160 °C, with initial monomer content of 40 wt%. Solid, dashed, dash–dotted and dotted lines represent model predictions for oxygen-initiated, DTBP-initiated, DCP-initiated and TBPC-initiated polymerization, with initial impurity amount of 800 ppm, at 160 °C and initial monomer content of 40 wt%.

Table 6
Activation energies of self-initiating monomers

Monomer	E (J mol^{-1})	Monomer content[a] (wt%)	Ref.
*n*BA	73,152	33	This study
MMA	85,600[b]	50	[27]
Styrene	108,500	100	[39]

[a] Initial monomer content at 170 °C, ca. 20 min reaction time, 30% monomer conversion.
[b] Based on the postulated participation of molecular oxygen in the self-initiation mechanism.

5.3. Spontaneous initiation mechanism

While this study reports the estimated rate constant for self-initiation, direct evidence for self-initiation is still absent. Thus we also consider the possibility of initiation by decomposition of impurities (e.g. oxygen and peroxides). The Arrhenius expressions reported by [30] are used to represent rate of decomposition of common peroxides (Table 5). In Fig. 8, two cases are considered: (i) in the case that an unknown amount impurities initiate the polymerization and the decomposition rate is approximately equal to the decomposition rate of molecular oxygen, and (ii) when the amount of impurities is known, however, the rate at which they decompose is not known. The first plot (top plot, Fig. 8) shows that trace amount of impurities, ca. 800 ppm, is able to initiate and sustain a considerable rate of polymerization, with a slow rate of impurity decomposition. It should be noted, however, that solubility of oxygen in organic medium is well below 800 ppm. Hence, the hypothetical scenario of oxygen-initiated polymerization (in conjunction with the reported secondary constants) is deemed unrealistic. The second plot (bottom plot, Fig. 8) shows that faster impurity decomposition rates lead to lower final monomer conversion. Thus much higher amounts $\gg$800 ppm, of impurities with faster decomposition rates, need to be present to initiate and sustain observed monomer conversion profiles.

From the reported estimates, we are also able to analyze the activation energy of the postulated second-order self-initiation, by comparing the estimated activation energy for *n*-butyl acrylate with other self-initiating monomers. The comparison is presented in Table 6. Note that the amount of initial monomer required to achieve 30% monomer conversion in ca. 20 min reaction time at 170 °C, increases with increasing energy of activation. In other words, the lower the initial monomer content required to achieve a certain degree of monomer conversion (at a given temperature and reaction time) the lower the activation energy associated with the self-initiation reaction. Thus the observed trend of the self-initiation activation energy and the high amount of impurities required to obtain observed conversion profiles suggest the occurrence of self-initiation. However, at the moment there is still no direct evidence for self-initiation. It should also be noted that removal of oxygen/peroxide-type impurities through nitrogen bubbling of solvent prior to monomer feed, might not be adequate [37].

A more direct approach toward identifying the initiating molecules or quantifying amount of impurities will be presented in a future study.

6. Conclusions

A mechanistic model for high-temperature batch polymerization of *n*BA was developed and presented. The model was able to capture the process dynamics between 140 and 180 °C and between 20 and 40 wt%. Quality of estimated rate constants, along with the predictive capabilities of the developed model, is presented and discussed. New experimental observations that support previous studies on high-temperature solution of alkyl acrylates are also presented. This study sheds light on the nature of the spontaneous initiation, backbiting, β-scission and branch formation reaction mechanisms. It should also be noted that there are limitations to the extents by which extrapolations can be made based on the reported parameters. Future research directions in this field include: (i) identification of novel 'experimental sensors' or measurements for parameter estimation studies, (ii) design of experiments that provide direct evidence of self initiation (e.g. better impurity removal techniques), (iii) development of efficient parameter estimation approaches and (iv) development of iterative and data-driven approaches towards identification of polymerization reaction networks and the corresponding rate constants.

Acknowledgements

This study was supported in part by du Pont Marshall Laboratory and the National Science Foundation Grant CTS-0216837. The authors thank two anonymous reviewers for their insightful comments, and also the du Pont Marshall Laboratory NMR spectroscopists Tom Scholz and Mark Karalis for their invaluable help with the polymer characterization work, the process operators Peter Markos, Mike Rullo and Mike Darczuk for carrying out the batch polymerization experiments, and the Drexel undergraduate co-op students Amutha Jeyarajasingam and Erik Amrine for their help with the recipe implementations. Any opinions, findings, conclusions or recommendations expressed in this material are those of the authors and do not necessarily reflect the views of the National Science Foundation or E. I. du Pont de Nemours and Company.

Appendix A. Derivation of the batch polymerization process model

A.1. Rate laws for small molecules

Rate laws for dimers, oxygen and radical, xylol radical, monomer, solvent and micro-structural properties such as short chain-branching points (SCBs) and terminal double bonds (TDBs) were derived based on the postulated reaction network presented in Section 3. They are:

$$r_{\mathrm{M}} = -2k_{\mathrm{ti}}[M]^2 - k_{\mathrm{p}}[M]\left(P_0 + P_1 + P_2 + P_1^{\mathrm{TDB}} + \sum_{n=3}^{\infty} P_n\right) - k_{\mathrm{pq}}[M]\sum_{n=3}^{\infty} Q_n - k_{\mathrm{tm}}[M]\sum_{n=3}^{\infty} P_n \tag{A1}$$

$$r_{\mathrm{S}} = -k_{\mathrm{ts}}[S]\sum_{n=3}^{\infty} P_n$$

$$r_{\mathrm{R_1OOR_2}} = -k_{\mathrm{O_2}}[\mathrm{R_1OOR_2}]$$

$$r_{\mathrm{SCB}} = k_{\mathrm{pq}}[M]\sum_{n=3}^{\infty} Q_n$$

$$r_{\mathrm{TDB}} = k_{\beta}\sum_{n=3}^{\infty} Q_n + k_{\mathrm{p}}[M]P_1^{\mathrm{TDB}}$$

$$r_{P_0} = 2k_{\mathrm{R_1OOR_2}}[\mathrm{R_1OOR_2}] + k_{\mathrm{ts}}[S]\sum_{n=3}^{\infty} P_n - k_{\mathrm{p}}[M]P_0$$

$$r_{P_1} = 2k_{\mathrm{ti}}[M]^2 + k_{\mathrm{p}}^{\mathrm{sec}}[M]R_0^{\mathrm{L}} - k_{\mathrm{p}}^{\mathrm{sec}}[M]R_1^{\mathrm{L}}$$

$$r_{P_2} = k_{\beta}\sum_{n=3}^{\infty} Q_n + k_{\mathrm{p}}[M]P_1^{\mathrm{TDB}} + k_{\mathrm{p}}[M]P_1 - k_{\mathrm{p}}[M]P_2$$

$$r_{P_1^{\mathrm{TDB}}} = k_{\mathrm{tm}}[M]\sum_{n=3}^{\infty} P_n - k_{\mathrm{p}}[M]P_1^{\mathrm{TDB}}$$

A.2. Rate laws for 'live' and 'dead' polymer chains

Rate laws for live secondary propagating radicals, live tertiary propagating radicals and dead chains of length *n*, based on postulated reaction network presented in Section 3, take the following form

$$r_{P_n} = k_{\mathrm{p}}[M](P_{n-1} - P_n) + k_{\mathrm{pq}}[M]Q_{n-1} - (k_{\mathrm{bb}} + k_{\mathrm{tm}}[M] + k_{\mathrm{ts}}[S])P_n - 2\left(k_{\mathrm{tc}}^{sec-sec} + k_{\mathrm{td}}^{sec-sec}\right)P_n\sum_{m=3}^{\infty} P_m - \left(k_{\mathrm{tc}}^{sec-tert} + k_{\mathrm{td}}^{sec-tert}\right)P_n\sum_{m=3}^{\infty} Q_m \tag{A2}$$

$$r_{Q_n} = k_{\mathrm{bb}}P_n - (k_{\mathrm{pq}}[M] + k_{\beta})Q_n - 2\left(k_{\mathrm{tc}}^{tert-tert} + k_{\mathrm{td}}^{tert-tert}\right)Q_n\sum_{m=3}^{\infty} Q_m - \left(k_{\mathrm{tc}}^{sec-tert} + k_{\mathrm{td}}^{sec-tert}\right)Q_n\sum_{m=3}^{\infty} P_m$$

$$r_{D_n} = (k_{tm}[M] + k_{ts}[S])P_n + k_\beta Q_{n+2} + k_{tc}^{sec-sec}\sum_{m=3}^{\infty} P_{n-m}P_m + k_{tc}^{sec-tert}\sum_{m=3}^{\infty} P_{n-m}Q_m + k_{tc}^{sec-tert}\sum_{m=3}^{\infty} Q_{n-m}P_m + k_{tc}^{tert-tert}\sum_{m=3}^{\infty} Q_{n-m}Q_m + 2k_{td}^{sec-sec}P_n\sum_{m=3}^{\infty} P_m + 2k_{td}^{sec-tert}P_n\sum_{m=3}^{\infty} Q_m + 2k_{td}^{sec-tert}Q_n\sum_{m=3}^{\infty} P_m + 2k_{td}^{tert-tert}Q_n\sum_{m=3}^{\infty} Q_m$$

The kth moment of the live and dead chains were defined as:

$$\lambda_k = \sum_{n=3}^{\infty} n^k P_n$$

$$\delta_k = \sum_{n=3}^{\infty} n^k Q_n$$

$$\mu_k = \sum_{n=3}^{\infty} n^k D_n$$

When the above moment definitions were applied to the rate laws, the following equations were obtained;

$$r_M = -2k_{ti}[M]^2 - k_p[M](P_0 + P_1 + P_2 + P_1^{TDB} + \lambda_0) - k_{pq}[M]\delta_0 - k_{tm}[M]\lambda_0 \quad (A3)$$

$$r_S = -k_{ts}[S]\lambda_0$$

$$r_{R_1OOR_2} = -k_{O_2}[R_1OOR_2]$$

$$r_{SCB} = k_{pq}[M]\delta_0$$

$$r_{TDB} = k_\beta\delta_0 + k_p[M]P_1^{TDB}$$

$$r_{P_0} = 2k_{O_2}[R_1OOR_2] + k_{ts}[S]\lambda_0 - k_p[M]P_0$$

$$r_{P_1} = 2k_{ti}[M]^2 + k_p[M]P_0 - k_p[M]P_1$$

$$r_{P_2} = k_\beta\delta_0 + k_p[M]P_1^{TDB} + k_p[M]P_1 - k_p[M]P_2$$

$$r_{P_1^{TDB}} = k_{tm}[M]\lambda_0 - k_p[M]P_1^{TDB}$$

$$r_{\lambda_0} = k_p[M]P_2 + k_{pq}[M]\delta_0 - (k_{bb} + k_{tm}[M] + k_{ts}[S])\lambda_0 - 2\left(k_{tc}^{sec-sec} + k_{td}^{sec-sec}\right)(\lambda_0)^2 - \left(k_{tc}^{sec-tert} + k_{td}^{sec-tert}\right)\lambda_0\delta_0 \quad (A4)$$

$$r_{\delta_0} = k_{bb}\lambda_0 - (k_{pq}[M] + k_\beta)\lambda_0 - 2\left(k_{tc}^{tert-tert} + k_{td}^{tert-tert}\right)(\delta_0)^2 - \left(k_{tc}^{sec-tert} + k_{td}^{sec-tert}\right)\lambda_0^L\lambda_0^{SCB}$$

$$r_{\mu_0} = (k_{tm}[M] + k_{ts}[S])\lambda_0^L + k_\beta\lambda_0^{SCB} + (k_{tc}^{sec-sec} + 2k_{td}^{sec-sec})(\lambda_0^L)^2 + (2k_{tc}^{sec-tert} + 4k_{td}^{sec-tert})\lambda_0^L\delta_0^{SCB} + (k_{tc}^{tert-tert} + 2k_{td}^{tert-tert})(\lambda_0^{SCB})^2$$

$$r_{\lambda_1} = k_p[M](P_2 + \lambda_0) + k_{pq}[M]\delta_1 - (k_{bb} + k_{tm}[M] + k_{ts}[S])\lambda_1 - 2(k_{tc}^{sec-sec} + k_{td}^{sec-sec})\lambda_0\lambda_1 - (k_{tc}^{sec-tert} + k_{td}^{sec-tert})\lambda_1\delta_0 \quad (A5)$$

$$r_{\delta_1} = k_{bb}\lambda_1 - (k_{pq}[M] + k_\beta)\delta_1 - 2(k_{tc}^{tert-tert} + k_{td}^{tert-tert})\delta_1\delta_0 - (k_{tc}^{sec-tert} + k_{td}^{sec-tert})\lambda_0\delta_1$$

$$r_{\mu_1} = (k_{tm}[M] + k_{ts}[S])\lambda_1 + k_\beta\delta_1 + 2k_{tc}^{sec-sec}(\lambda_0\lambda_1) + 2k_{tc}^{sec-tert}(\lambda_0\delta_1 + \lambda_1\delta_0) + 2k_{td}^{tert-tert}(\delta_0\delta_1) + 2k_{td}^{sec-sec}\lambda_0\lambda_1 + 2k_{td}^{sec-tert}(\lambda_1\delta_0 + \lambda_0\delta_1) + 2k_{tc}^{tert-tert}(\delta_0\delta_1)$$

$$r_{\lambda_2} = k_p[M](P_2 + \lambda_0 + 2\lambda_1) + k_{pq}[M]\delta_2 - (k_{bb} + k_{tm}[M] + k_{ts}[S])\lambda_2 - 2(k_{tc}^{sec-sec} + k_{td}^{sec-sec})\lambda_0\lambda_2 - (k_{tc}^{sec-tert} + k_{td}^{sec-tert})\lambda_2\delta_0 \quad (A6)$$

$$r_{\delta_2} = k_{bb}\lambda_2 - (k_{pq}[M] + k_\beta)\delta_2 - 2(k_{tc}^{tert-tert} + k_{td}^{tert-tert})\delta_2\delta_0 - (k_{tc}^{sec-tert} + k_{td}^{sec-tert})\lambda_0\delta_2$$

$$r_{\mu_2} = (k_{tm}[M] + k_{ts}[S])\lambda_2 + k_\beta\delta_2 + 2k_{tc}^{sec-sec}[\lambda_0\lambda_2 + (\lambda_1)^2] + 2k_{tc}^{sec-tert}(\lambda_0\delta_2 + 2\lambda_1\delta_1 + \lambda_2\delta_0) + 2k_{tc}^{tert-tert}(\delta_0\delta_2 + (\delta_1)^2] + 2k_{td}^{sec-sec}\lambda_0\lambda_2 + 2k_{td}^{sec-tert}(\lambda_2\delta_0 + \lambda_0\delta_2) + 2k_{td}^{tert-tert}(\delta_0\delta_2)$$

A.3. Batch process model

The rate laws were then incorporated in conservation (balance) equations for a batch polymerization reactor model. Perfect mixing and constant volume (negligible volume changes in reaction medium during reaction time) were assumed. Quasi steady-state assumption on the live chains is not made. The batch polymerization reactor model is of the form;

$$\frac{d[M]}{dt} = r_M, \quad [M](0) = [M]_0 \quad (A7)$$

$$\frac{d[S]}{dt} = r_S, \quad [S](0) = [S]_0$$

$$\frac{d[R_1OOR_2]}{dt} = r_{R_1OOR_2}, \quad [R_1OOR_2](0) = [R_1OOR_2]_0$$

$$\frac{d[TDB]}{dt} = r_{TDB}, \quad [TDB](0) = 0$$

$$\frac{d[SCB]}{dt} = r_{SCB}, \quad [SCB](0) = 0$$

$$\frac{d[P_0]}{dt} = r_{P_0}, \quad [P_0](0) = 0$$

$$\frac{d[P_1]}{dt} = r_{P_1}, \quad [P_1](0) = 0$$

$$\frac{d[P_2]}{dt} = r_{P_2}, \quad [P_2](0) = 0$$

$$\frac{d[P_1^{TDB}]}{dt} = r_{P_1^{TDB}}, \quad [P_1^{TDB}](0) = 0$$

$$\frac{d\lambda_k}{dt} = r_{\lambda_k}, \quad \lambda_k(0) = 0,\ k = 0, 1, 2$$

$$\frac{d\delta_k}{dt} = r_{\delta_k}, \quad \delta_k(0) = 0,\ k = 0, 1, 2$$

$$\frac{d\mu_k}{dt} = r_{\mu_k}, \quad \mu_k(0) = 0,\ k = 0, 1, 2$$

The measured variables are related to the state variables of the preceeding model according to:

$$M_n = \frac{\mu_1}{\mu_0} MW_m \quad TDBH = \frac{[TDB]}{\mu_1} \times 100 \tag{A8}$$

$$M_w = \frac{\mu_2}{\mu_1} MW_m \quad SCBH = \frac{[SCB]}{\mu_1} \times 100$$

$$X = 1 - \frac{[M]}{[M](0)} \quad TSGH = \frac{[S]_0 - [S]}{\mu_1} \times 100$$

References

[1] Grady MC, Simonsick WJ, Hutchinson RA. Studies of higher temperature polymerization of *n*-butyl methacrylate and *n*-butyl acrylate. Macromol Symp 2002;182:149–68.

[2] Peck ANF, Hutchinson RA. Secondary reactions in the high-temperature free radical polymerization of butyl acrylate. Macromolecules 2004;37: 5944–51.

[3] Ahmad NM, Heatley F, Lovell PA. Chain transfer to polymer in free-radical solution polymerization of *n*-butyl acrylate studied by NMR spectroscopy. Macromolecules 1998;31:2822–7.

[4] Chiefari J, Jeffery J, Mayadunne RTA, Moad G, Rizzardo E, Thang SH. Chain transfer to polymer: a convenient route to macromonomers. Macromolecules 1999;32:7700–2.

[5] McCord EF, Shaw Jr WH, Hutchinson RA. Short-chain branching structures in ethylene copolymers prepared by high-pressure free-radical polymerization: an NMR analysis. Macromolecules 1997;30:246–56.

[6] Peck ANF, Hutchinson RA, Grady MC. Branching and scission reactions in high temperature acrylate polymerizations. Polym Prepr 2002;43: 154–5.

[7] Fernandez-Garcia M, Fernandez-Sanz M, Madruga EL. A kinetic study of butyl acrylate free radical polymerization in benzene solution. Macromol Chem Phys 2000;201:1840–5.

[8] Asua JM, Beuermann S, Buback M, Castignolles P, Charleux B, Gilbert RG, et al. Critically evaluated rate coefficients for free-radical polymerization, 5. Propagation rate coefficient for butyl acrylate. Macromol Chem Phys 2004;205:2151–60.

[9] Nikitin AN, Castignolles P, Charleux B, Vairon JP. Determination of propagation rate coefficient of acrylates by pulsed-laser polymerization in the presence of intramolecular chain transfer to polymer. Macromol Rapid Commun 2003;24:778–82.

[10] Buback M, Egorov M, Feldermann A. Chain-length dependence of termination rate coefficients in acrylate and methacrylate homopolymerizations investigated via the sp-plp technique. Macromolecules 2004;37: 1768–76.

[11] Beuermann S, Buback M. Rate coefficients of free-radical polymerization deduced from pulsed laser experiments. Prog Polym Sci 2002;27: 191–254.

[12] Busch M, Muller M. Simulating acrylate polymerization reactions: toward improved mechanistic understanding and reliable parameter estimates. Macromol Symp 2004;206:399–418.

[13] Polic AL, Lona LMF, Duever TA, Penlidis A. A protocol for the estimation of parameters in process models: case studies with polymerization scenarios. Macromol Theory Simul 2004;13:115–32.

[14] Li RJ, Henson MA, Kurtz MJ. Selection of model parameters for off-line parameter estimation. IEEE Trans Control Syst Technol 2004;12:402–12.

[15] Wulkow M. The simulations of molecular weight distributions in polyreaction kinetics by discrete galerkin methods. Macromol Theory Simul 1996;5:393–416.

[16] Grady MC, Quan C, Soroush C. Thermally initiated polymerization process for acrylates. US Patent Appl. Publ. US20050003094; 2005 p. 7.

[17] Quan C, Soroush M, Grady MC, Hansen JE, Simonsick Jr WJ. High-temperature homopolymerization of ethyl acrylate and *n*-butyl acrylate: polymer characterization. Macromolecules 2005;38:7619–28.

[18] Stickler M, Meyerhoff G. Thermal polymerization of methyl methacrylate, 1. Polymerization in bulk. Makromol Chem 1978;179:2729–45.

[19] Brand E, Stickler M, Meyerhoff G. Spontaneous polymerization of methyl methacrylate, 3. Reaction behavior of the unsaturated dimer upon polymerization. Makromol Chem 1980;181:913–21.

[20] Lingnau J, Stickler M, Meyerhoff G. The spontaneous polymerization of methyl methacrylate. IV. Formation of cyclic dimers and linear trimers. Eur Polym J 1980;16:785–91.

[21] Stickler M, Meyerhoff G. The spontaneous thermal polymerization of methyl methacrylate. 5. Experimental study and computer simulation of the high conversion reaction at 130 C. Polymer 1981;22:928–33.

[22] Lingnau J, Stickler M, Meyerhoff G. The spontaneous polymerization of methyl methacrylate. 6. Polymerization in solution: participation of transfer agents in the initiation reaction. Polymer 1983;24:1473–8.

[23] Lingnau J, Meyerhoff G. The spontaneous polymerization of methyl methacrylate, 7. External heavy atom effect on the initiation. Makromol Chem 1984;185:587–600.

[24] Lingnau J, Meyerhoff G. Spontaneous polymerization of methyl methacrylate. 8. Polymerization kinetics of acrylates containing chlorine atoms. Macromolecules 1984;17:941–5.

[25] Clouet G, Chaumont P, Corpart P. Studies on bulk-polymerization of methyl-methacrylate. 1. Thermal polymerization. J Polym Sci, Part A: Polym Chem 1993;31:2815–24.

[26] Lehrle RS, Shortland A. A study of the purification of methyl methacrylate suggests that the 'thermal' polymerisation of this monomer is initiated by adventitious peroxides. Eur Polym J 1988;24:425–9.

[27] Nising P, Meyer T, Carloff R, Wicker M. Thermal initiation of mma in high temperature radical polymerizations. Macromol Mater Eng 2005; 290:311–8.

[28] McManus NT, Penlidis A, Dube MA. Copolymerization of alpha-methyl styrene with butyl acrylate in bulk. Polymer 2002;43:1607–14.

[29] Cao G, Zhu Z, Zhang M, Yuan W. Kinetics of butylacrylate polymerization in a starved feed reactor. J Appl Polym Sci 2004;93: 1319–525.
[30] Cerinski B, Jelencic J. Modeling of high-pressure ethylene polymerization. I. Kinetic parameters of oxygen initiation. J Appl Polym Sci 2002; 83:2043–51.
[31] Willemse RXE, van Herk AM, Panchenko E, Junkers T, Buback M. Plp-esr monitoring of midchain radicals in *n*-butyl acrylate polymerization. Macromolecules 2005;38:5098–103.
[32] Maeder S, Gilbert RG. Measurement of transfer constant for butyl acrylate free radical polymerization. Macromolecules 1998;31:4410–8.
[33] Raghuram PVT, Nandi US. Studies on the polymerization of ethyl acrylate. II. Chain transfer studies. J Polym Sci Part A-1 1969;7: 2379–85.
[34] Odian GG. Principles of polymerization. 3rd ed. Hoboken, NJ, USA: Wiley; 1991.
[35] Vana P, Davis TP, Barner-Kowollik C. End-group analysis of polymers by electrospray ionization mass spectrometry: 2-methyl-1-[4-(methylthio)phenyl]-2-morpholinopropan-1-one initiated free-radical photopolymerization. Aust J Chem 2002;55:315–8.
[36] Buback M, Egorov M, Gilbert RG, Kaminsky V, Olaj OF, Russell GT, et al. Critically evaluated termination rate coefficients for free-radical polymerization, 1-the current situation. Macromol Chem Phys 2002;203:2570–82.
[37] Albertin L, Stenzel MH, Barner-Kowollik C, Foster LJR, Davis TP. Solvent and oxygen effects on the free radical polymerization of 6-o-vinyladipoyl-d-glucopyranose. Polymer 2005;46:2831–5.
[38] Plessis C, Arzamendi G, Alberdi JM, van Herk AM, Leiza JR, Asua JM. Evidence of branching in poly(butyl acrylate) produced in pulsed-laser polymerization experiments. Macromol Rapid Commun 2003;24:173–7.
[39] Hui AW, Hamielec AE. Thermal polymerization of styrene at high conversions and temperatures. Experimental study. J Appl Polym Sci 1972;16:749–69.